ISSN 1063-7729, Astronomy Reports, 2019, Vol. 63, No. 1, pp. 66–78. © Pleiades Publishing, Ltd., 2019.
Russian Text © E.V. Atkin, V.L. Bulatov, O.A. Vasiliev, A.G. Voronin, N.V. Gorbunov, V.M. Grebenyuk, V.A. Dorokhov, D.E. Karmanov, I.M. Kovalev, I.A. Kudryashov, A.A. Kurganov, M.M. Merkin, A.D. Panov, D.M. Podorozhny, D.A. Polkov, S.Yu. Porokhovoi, L.G. Sveshnikova, L.G. Tkachev, A.V. Tkachenko, A.N. Turundaevskiy, S.B. Filippov, V.V. Shumikhin, 2019, published in Astronomicheskii Zhurnal, 2019, Vol. 96, No. 1, pp. 75–88.

Energy Spectra of Cosmic-Ray Protons and Nuclei Measured in the NUCLEON Experiment Using a New Method

E. V. Atkin[1], V. L. Bulatov[2], O. A. Vasiliev[3], A. G. Voronin[3], N. V. Gorbunov[4], V. M. Grebenyuk[4], V. A. Dorokhov[2], D. E. Karmanov[3], I. M. Kovalev[3], I. A. Kudryashov[3], A. A. Kurganov[3], M. M. Merkin[3], A. D. Panov[3], D. M. Podorozhny[3], D. A. Polkov[2], S. Yu. Porokhovoi[4], L. G. Sveshnikova[3], L. G. Tkachev[4], A. V. Tkachenko[4], A. N. Turundaevskiy[3*], S. B. Filippov[2], and V. V. Shumikhin[1]

[1] *Moscow Engineering Physics Institute, National Nuclear Research Institute, Moscow, Russia*

[2] *OOO "Gorizont", Yekaterinburg, Russia*

[3] *Skobel'tsyn Institute of Nuclear Physics, Lomonosov Moscow State University, Moscow, 119234 Russia*

[4] *Joint Institute for Nuclear Research, Dubna, Moscow region, 141980 Russia*

Received May 25, 2018; in final form, June 22, 2018

Abstract—Some results of studies of cosmic rays obtained during the NUCLEON space experiment in 2015–2017 are presented. This experiment was intended for direct measurements of the energy spectra and chemical composition of cosmic rays ($Z = 1–30$) in the energy range 2–500 TeV. Results presented include energy spectra for various abundant nuclei measured using the new Kinematic Lightweight Energy Meter (KLEM). The primary energies are established using the spatial densities of secondary particles produced in inelastic interactions with a carbon target.

DOI: 10.1134/S1063772919010013

1. INTRODUCTION

The energy range $10^{14}–10^{16}$ eV preceding the "knee" is very important for studies of the acceleration and propagation of cosmic rays. More data with per element resolution are needed. No direct measurements of the spectra of cosmic-ray nuclei in the vicinity of the "knee" are available. The main information about cosmic-ray nuclei at energies of $10^{12}–10^{14}$ eV has been obtained from balloons (ATIC [1, 2], CREAM [3, 4], TRACER [5]) and satellites (AMS02 [6, 7] for lower energies, SOKOL [8]). The CALET experiment [9] is currently being carried out on board the International Space Stateion. The DAMPE experiment is also being conducted [10]. However, additional direct measurements at energies up to 1000 TeV are needed. A large geometrical factor is required for effective measurements of cosmic-ray fluxes at high energies.

A new kinematic method for measuring the energies of protons and nuclei, the Kinematic Lightweight Energy Meter, KLEM, was recently proposed [11]. This makes it possible to realize spectrometers with large geometrical factors and low masses. The NUCLEON space experiment is intended for direct, out-of-atmosphere studies of the energy spectra and chemical composition of cosmic rays from 2 TeV to more than 500 TeV (up to the "knee"). The highest measured energy is 900 TeV.

2. CONSTRUCTION OF THE NUCLEON INSTRUMENT

NUCLEON [11–16] was developed through a collaboration of the Skobel'tsyn Institute of Nuclear Physics of Lomonosov Moscow State University, the Joint Institute for Nuclear Research in Dubna, and a number of other Russian scientific and industrial centers. The instrument is currently on board the RESURS-P No. 2 satellite. The spacecraft orbit is sun-synchronous with an inclination of 97.276° and a mean altitude of 475 km. The spacecraft was launched on December 26, 2014. The scientific goals of the experiment and the methods applied determined the structure of the installation. An overview of the NUCLEON instrument is presented in Fig. 1. The new kinematic method realized through KLEM was used for energy measurements for the first time [11].

NUCLEON includes various systems based on silicon and scintillator detectors [11] designed for

*E-mail: turun1966@yandex.ru

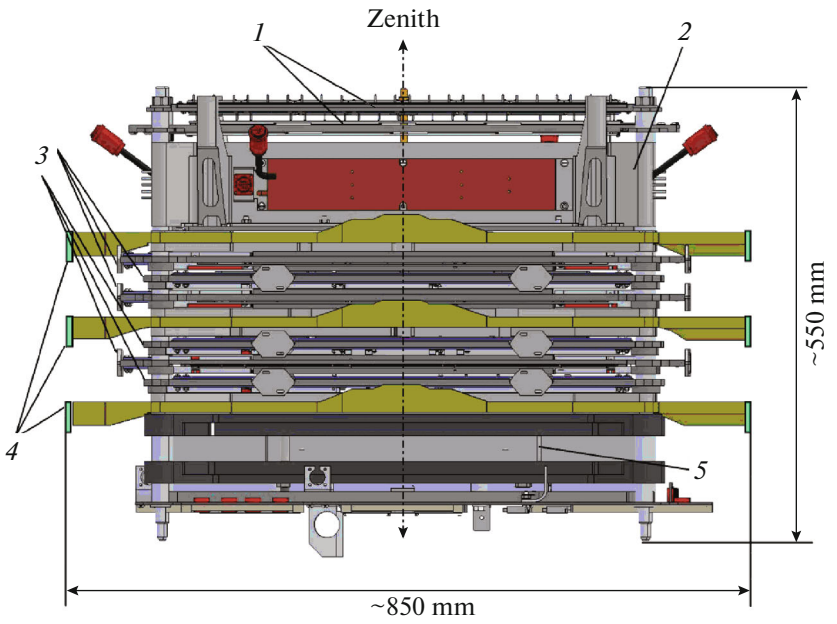

Fig. 1. (Color online) Simplified schematic of the NUCLEON apparatus. (*1*) Two pairs of planes for the charge-measurement system; (*2*) carbon target; (*3*) six planes of the KLEM energy-measurement system; (*4*) three layers of the trigger system; (*5*) calorimeter.

measurements of charge and energy. The total mass of the instrument is about 375 kg. The effective geometrical coefficient is more than 0.2 m^2 sr for the KLEM system and about 0.06 m^2 sr for the calorimeter. The operational area of the installation is 0.25 m^2. The charge-measurement system has a resolution of 0.15–0.20 charge units.

We present the results of measurements obtained over about three years, during 2015–2017. Table 1 compares the total exposure factor for NUCLEON with those for other experiments aimed at directly measuring the spectra of high-energy cosmic rays. The data obtained by all these detectors can be considered images of events. An example of an event is presented in Fig. 2. The reconstructed trajectory intersects the charge detector (1), the KLEM silicon microstrip detector systems for measuring energy (3), and the silicon microstrip detectors in the ionizational calorimeter (5). The projections obtained can be used to establish the direction and other characteristics of a cascade in the installation.

3. THE KLEM METHOD

The KLEM new kinematic method for measuring energy was proposed in [17–21]. This method can be applied over a wide range of energies (10^{11}–10^{16} eV) and has an energy resolution of 70% or better, according to the results of mathematical simulation [13, 15, 16, 22].

The simple kinematic method proposed by Castagnoli et al. [23] has large uncertainties (100–200%). A combined method was proposed to enhance the resolution [17–21], taking into account the characteristics of high-energy inelastic hadronic interactions. The method of [23] was based on the assumption that the secondary pions in proton interactions emerge symmetrically forward and backward in the center of mass system of the colliding particles. In this case, due to the Lorentz transformation, the mean value of the pseudorapidity in the laboratory frame, $\eta = -\ln\tan(\theta_i/2)$, where θ_i is the angle at which the secondary particle leaves, is proportional to the logarithm of the primary energy of the incident particle. This method has been applied in experiments where nuclear emulsions and spark chambers were used as detectors; this did not enable the registration of secondary gamma-rays formed from the decay of neutral pions and led to violation of the condition that the charged particles emerge symmetrically in the center-of-mass system of the colliding protons (since the gamma-rays carry an unknown fraction of the momentum). In addition, in nucleon–nucleus interactions, the left wing of the pseudorapidity density function $dN/d\eta$ is distorted by the contribution of particles formed in subsequent interactions between the incident nucleon and nucleons in the target, which enhances fluctuations of $dN/d\eta$ in indiviual events, and thus increases the uncertainty in the energy. These factors and the difficulties in experimentally registering particles in the back cone were

Table 1. Experiments on direct measurements of high-energy cosmic-ray spectra

Experiment	Range	Exposure factor m^2 sr year
NUCLEON	>2 TeV	0.7 (2015–2017)
ATIC (balloon)	>50 GeV	0.04
CREAM (balloon)	>2.5 TeV	0.35 (3 flights)
TRACER (balloon)	>0.5 GeV/n	0.25 (2 flights)
AMS02	<2 TV	5 (expected)
DAMPE	>100 GeV	1 (expected)
CALET	>1 GeV	0.5 (expected)
ISS-CREAM	>1 TeV	3 (expected)

the main reason for the very large uncertainties in the energies yielded by the method of Castagnoli et al. [23].

Given the difficulties in determining the energy from the flight angles of secondary particles described above, a combined method was proposed, based on measurements of the flight angles of the fastest charged and neutral particles, also using information abut the energies of secondary particles. Figure 1 shows that the instrument used for these measurements consists of a target and thin layers of dense material that play the role of gamma-ray converters. A layer of coordinate-sensitive detectors capable of fixing the number and coordinates of charged particles is placed beneath a converter.

The primary particle interacts in the target, where secondary gamma-rays and charged particles are produced. The particles after the converter include electrons and positrons produced in an electromagnetic cascade.

Mathematical simulation was used to identify the optimal estimator relating the spatial distribution of the charged particles after the converter and the primary energy of the incident particle. In practice, the spatial density of the secondary particles is registered by silicon microstrip detectors. The estimator S used in the data analysis is defined as

$$S = \sum_k I_k \ln^2(2H/x_k), \qquad (1)$$

where x_k is the distance between the shower axis and strip k, I_k the signal in strip k, and H the distance between the middle of the graphite target and the plane of the microstrip detectors. The mathematical modeling showed that the dependence $S(E)$ is close to a power law, and has nearly the same slope for different types of primary nuclei over a wide range of energies.

4. MATHEMATICAL SIMULATION

4.1. Simulations of the Energy Measurement System

Isotropic fluxes of protons and nuclei of helium, carbon, sulfur, and iron were simulated. To ensure statistical reliability over the entire energy range (100 GeV–1000 TeV), a uniform distribution in the logarithm of the primary energy was used, $dN/d(\ln E) = \text{const}$. The signals in the scintillators and silicon detectors were taken to be proportional to the energy release in the corresponding volume. Identical algorithms were used to process the simulated and experimental data. The trigger conditions and determination of the directions of the trajectories of primary particles were reproduced. The KLEM method was optimized for selected events, and the calibration curves calculated.

Simulations were carried out in order to estimate the practical suitability of the proposed energy-measurement method using the GEANT 3.21 software package [24] supplemented with the QGSJET generator [25, 26] to describe high-energy hadron–nucleus and nucleus–nucleus interactions.

4.2. Calibration Curves for Various Cosmic-Ray Components

The following main assumptions were used when analyzing the results of the mathematical modeling. A power-law dependence was assumed for the dependence of the recontructed energy on the estimator S:

$$E_{\text{rec}} = aS^b. \qquad (2)$$

Further, it was assumed that the distribution function of the reconstructed energy does not depend on the primary energy, only the ratio of the reconstructed

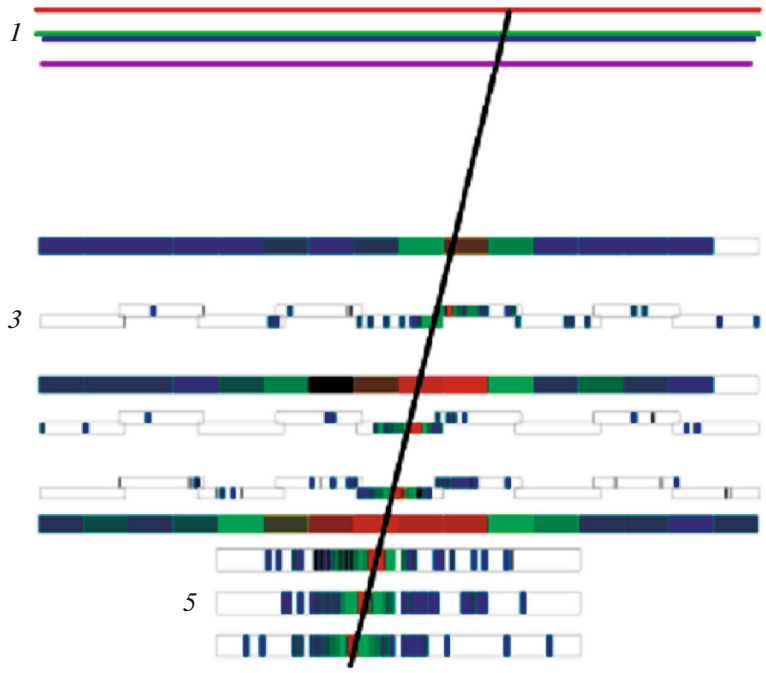

Fig. 2. (Color online) Image of an event. A nucleus has initiated a cascade. (*1*) Two pairs of planes in the charge-measurement system; (*3*) six planes of the KLEM energy-measurement system; (*5*) calorimeter.

and primary energies $F(E_{\rm rec}/E)$. Here, we will introduce the notation $k = E_{\rm rec}/E$. It is known that the shape of cosmic-ray spectra are close to power laws:

$$\frac{dN}{dE} = AE^{-(\gamma+1)}. \quad (3)$$

For a given reconstructed energy,

$$E = E_{\rm rec}/k. \quad (4)$$

We introduce the condition $\langle k\rangle = 1$ for the power-law energy spectrum. This leads to the equations

$$\frac{dN}{dk} = AE_{\rm rec}^{-\gamma}k^{\gamma}, \quad (5)$$

$$\langle k\rangle = \frac{\sum\limits_i k_i^{\gamma+1}}{\sum\limits_i k_i^{\gamma}} = 1. \quad (6)$$

We obtain for a simulated event with energy E_i

$$k_i = \frac{aS_i^b}{E_i}. \quad (7)$$

As a result, we obtain for the parameter a

$$a = \frac{\sum\limits_i (S_i^b/E_i)^{\gamma}}{\sum\limits_i (S_i^b/E_i)^{(\gamma+1)}}. \quad (8)$$

An ordinary least-squares method was used to derive the values of b for various components based on the simulated data. The values of a were calculated using the formula obtained above. Use of the resulting values of a and b makes it possible to obtain an unbiased estimate of the energy for a power-law spectrum. In practice, one can use the more convenient parameter a_2:

$$E_{\rm rec} = a_2(S\times 10^{-5})^b. \quad (9)$$

The values of a_2 and b are presented in Table 2. The simulation results for protons and carbon nuclei (S as a function of E) are presented in Fig. 3.

As was indicated above, in the simulations, the energy of the primary particles was assigned values having a uniform energy distribution on a logarithmic scale. The thin line in Fig. 3 corresponds to a simple power-law fit to these data. However, we must take into account the fact that the real energy spectra of

Table 2. Calibration parameters

Component	a_2, GeV	b
p	1651	1.36
He	2556	1.27
C	3514	1.18
S	4163	1.14
Fe	4362	1.12

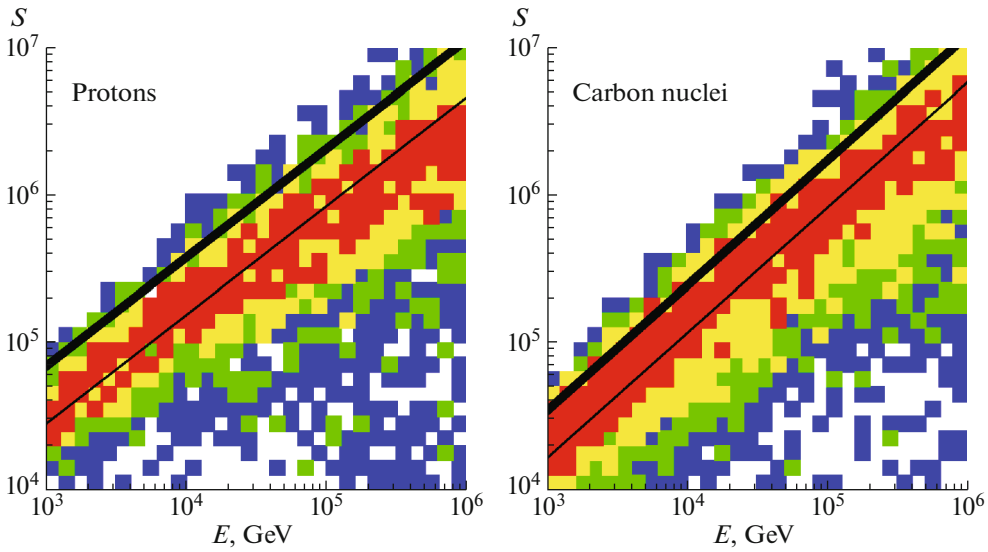

Fig. 3. (Color online) Simulation results: S versus E for protons and carbon nuclei. The fit shown by the thick line has been shifted taking into account the power-law spectrum. The thin line corresponds to a simple fit.

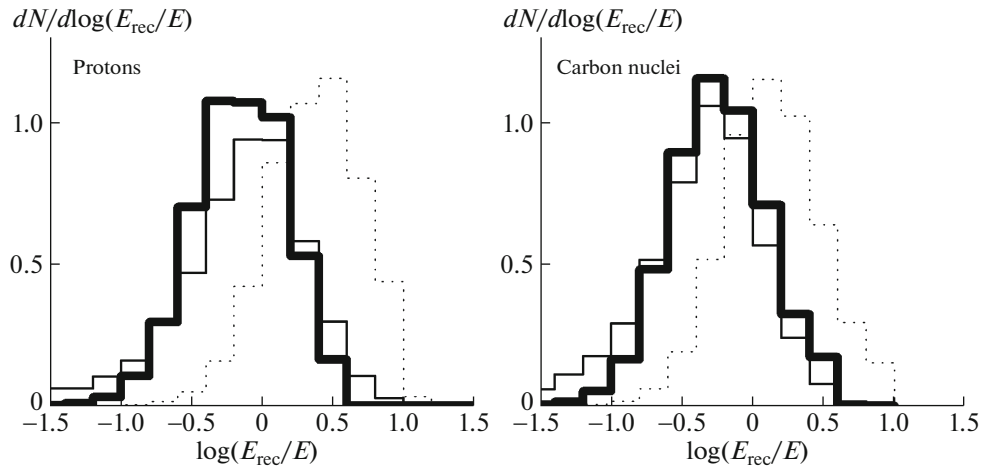

Fig. 4. Simulation results. Normalized reconstructed energy distributions for protons and carbon nuclei. The thin line corresponds to a simple fit to the data. The dotted line corresponds to the same fit with event weights corresponding to the real spectrum. The thick line corresponds to the distribution obtained by fitting with event weights corresponding to the real spectra.

cosmic rays are close to power laws. Thus, it is necessary to introduce weights for events in accordance with the expected energy spectra. The thick line in Fig. 3 corresponds to a power-law fit obtained with weighting coefficients in accordance with (8).

The normalized distributions for the reconstructed energy for the simulated events are presented in Fig. 4. Various approximations were used. The thin curve corresponds to a simple approximation, as in Fig. 3. This fit yields overestinated energies in a power-law spectrum. The dotted curve corresponds to a fit taking into account the weights of events for the real spectrum (the thick line in Figs. 3 and 4, fit parameters from Table 1).

The distribution of the reconstructed energy is a convolution of the distributions for fixed energies and the spectral shape. The energy resolution and registration efficiency depend on the spectral index.

4.3. Deconvolution of the Primary Spectra

The spectrum of the reconstructed energies obtained using the algorithm described above can be taken to be a first approximation for the true spectrum of the primary energies. We must reconstruct the energy spectrum of the primary particles from the spectrum for E_{rec} computed using the fits presented above.

Methods for deconvolving spectra were developed earlier for the analysis of data from the ATIC experiment [27, 28], and adapted for the NUCLEON experiment. Deconvolution with the regularization of Tikhonov [28] was applied in the processing of the NUCLEON data. The relationship between the spectrum of the reconstructed energies $f(E_{\rm rec})$ and the primary energy spectrum $\Phi(E)$ is described by an integral Fredholm equation of the first kind,

$$f(E_{\rm rec}) = \int A(E_{\rm rec}, E)\Phi(E)dE. \qquad (10)$$

Here, $A(E_{\rm rec}, E)$ is an instrumental function describing the distribution of the energy $E_{\rm rec}$ reconstructed using the estimator S for each primary energy E.

The experimental spectra are registered in terms of the number of counts in corresponding bins. The entire studied energy range is divided into n intervals, with the bin width being constant on a logarithmic scale. The integral equation can be rewritten in terms of a system of linear equations

$$M_i = \sum_{j=1}^{n} a_{ij}N_j, j = 1, 2, ..., n. \qquad (11)$$

Here, M_i is the number of events in bin i for the reconstructed energy, a_{ij} an element of the response matrix, and N_j the desired number of events of the primary spectrum in bin j. This system of linear equations can be solved via minimization of the function

$$F(N_1, ..., N_n) = \sum_{i=1}^{n} \left(\frac{\sum\limits_{j=1}^{n} a_{ij}N_j - M_i}{\sigma_i} \right)^2 \qquad (12)$$
$$+ \tau \sum_{j=2}^{n-1} \left(\frac{N_{j+1} - 2N_j + N_{j-1}}{\sigma_j} \right)^2 \to \min.$$

Here, σ_i is the standard deviation of M_i and τ is the regularization parameter [28]. The response matrix was calculated from the simulation results (Fig. 3), taking into account the power-law dependence $E_{\rm rec}(S)$. The energy-dependent registration efficiency for various nuclei and the exposure time were also taken into account.

The deconvolution of the energy spectra of the protons and helium nuclei leads to stable results. However, the statistics for nuclei with $Z \geq 6$ are insufficient to enable deconvolution of the spectra for each component. The differential-shift method was applied for these components, likewise developed for the ATIC experiment [27]. The primary energy for each bin was reconstructed in accordance with the expression

$$E_0^{(i)} = \frac{\sum\limits_{j=1}^{n} a_{ij}E_j K(E_j)}{\sum\limits_{j=1}^{n} a_{ij}K(E_j)}. \qquad (13)$$

Here, $K(E_j)$ is the initial power-law fit for the primary energy spectrum. We applied a direct deconvolution for the reconstruction of the proton and helium spectra. The spectra of other nuclei were reconstructed using the differential-shift method.

Accelerator tests of prototypes of the NUCLEON apparatus were carried out at the SPS accelerator at CERN [11, 13–15]. The results of ground experiments confirmed the applicability of the KLEM method.

5. RESULTS OF THE SPACE EXPERIMENT

5.1. Charge Measurements

The reduction of the data obtained from the spacecraft experiment includes several steps. In the first step, the particle trajectory is analyzed. For each layer of silidon microstrip detectors, the spatial position of the ionization maximum is located. It is assumed that these maxima correspond to the coordinates of the track at the level of the microstrip detector. An ordinary least-squares fit is used to reconstruct the axis from these points. Events outside the operational aperture of the installation were rejected.

The point where a particle passed through was determined from the charge measurements for each layer of silicon pad detectors. The coordinates of the pads around this point through which the primary particle could have passed were identified (taking into account the possible uncertainties). The signals from these pads were compared, and the pad with the highest amplitude was identified for each layer.

Calibration relations are needed to translate from registration of a signal amplitude in a measurement channel to determination of a charge. Results of tests of the apparatus using an ion beam were used in the first stage [14]. Possible drifts in the characteristics during flight were traced using on-board calibrations for each channel.

The initial calibrations were applied to construct first-level charge distributions with uncertainties of about 0.3–0.5 charge units. Further analysis showed that the main reason for these high uncertainties was the scatter of the characteristics of the various detectors in the charge-measurement system.

After accumulation of fairly good statistics (a half year of data), the charge distributions were constructed separately for each of the 256 detectors in the

Table 3. Statistical material for 2015–2017

Interval, GeV	p	He	C	O	Ne	Mg	Si	Fe	All nuclei
1×10^3–1.6×10^3	5632	10 653	4317	8180	1958	3183	3017	4112	49 009
1.6×10^3–2.5×10^3	3186	6106	2499	4781	1118	1981	2303	3490	30 953
2.5×10^3–4.0×10^3	1647	3455	1337	2354	518	934	1158	2578	17 324
4.0×10^3–6.3×10^3	904	1879	718	1139	271	448	518	1452	8867
6.3×10^3–1×10^4	471	1057	383	655	155	226	262	881	4739
1×10^4–1.6×10^4	219	505	180	337	67	101	142	299	2196
1.6×10^4–2.5×10^4	115	259	95	156	41	60	61	177	1115
2.5×10^4–4.0×10^4	42	139	42	66	23	18	39	61	515
4.0×10^4–6.3×10^4	22	48	25	37	3	16	17	40	247
6.3×10^4–1×10^5	9	32	10	12	5	1	8	18	111
1×10^5–1.6×10^5	3	10	6	9	3	2	3	4	46
1.6×10^5–2.5×10^5	0	3	1	2	1	1	0	1	11
2.5×10^5–4.0×10^5	1	0	0	0	1	0	0	0	3
4.0×10^5–6.3×10^5	0	0	0	0	0	0	0	0	1
6.3×10^5–1×10^6	0	1	0	0	0	0	0	0	1

charge-measurement system. Reference peaks from the most abundant nuclei, such as protons, helium, carbon, oxygen, and iron ($Z = 1, 2, 6, 8, 26$) were distinguished for each such distribution. Additional calibrations for each of the detectors were based on these peak values. Charge distributions with high resolution (0.15–0.20 for various nuclei, see Fig. 5) were obtained in this way. The modest shift of the charge peaks for $Z > 14$ is due to non-linearity of the electronics. This effect was also taken into account.

5.2. Reconstruction of the Energy Spectra

Both the energy dependence of the estimator S and the dependence of the registration efficiencies of the various components were taken into account when

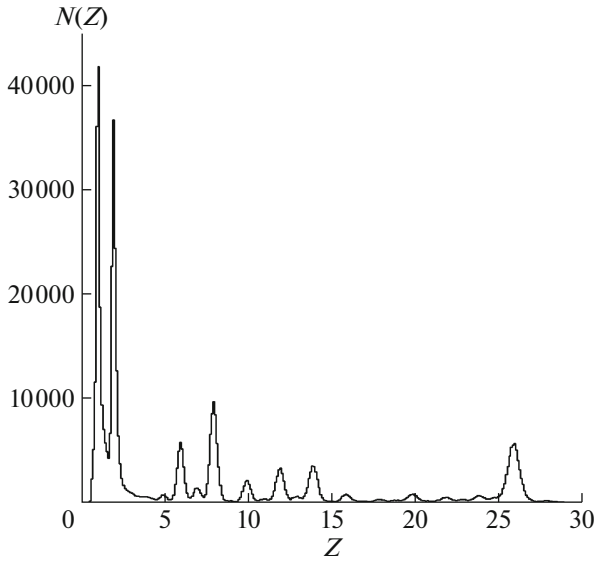

Fig. 5. Charge distribution in the NUCLEON experiment.

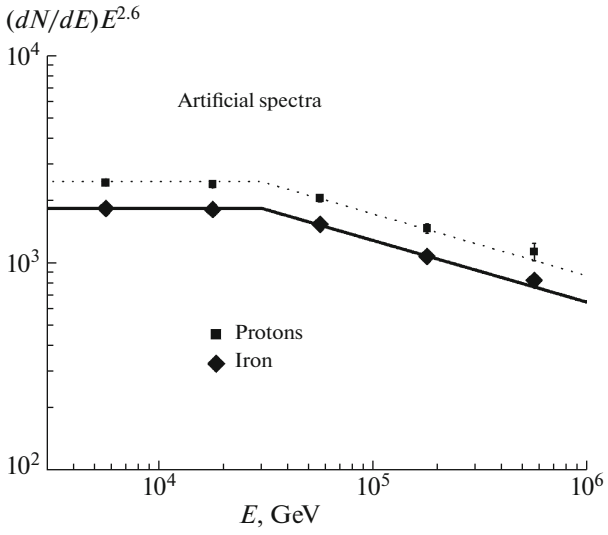

Fig. 6. Modeled (lines) and reconstructed (points) energy spectra.

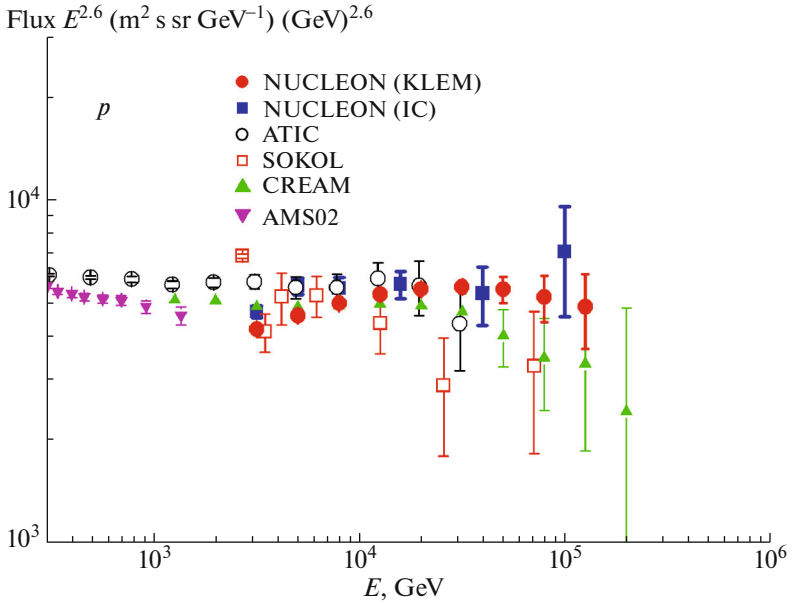

Fig. 7. (Color online) Proton spectrum.

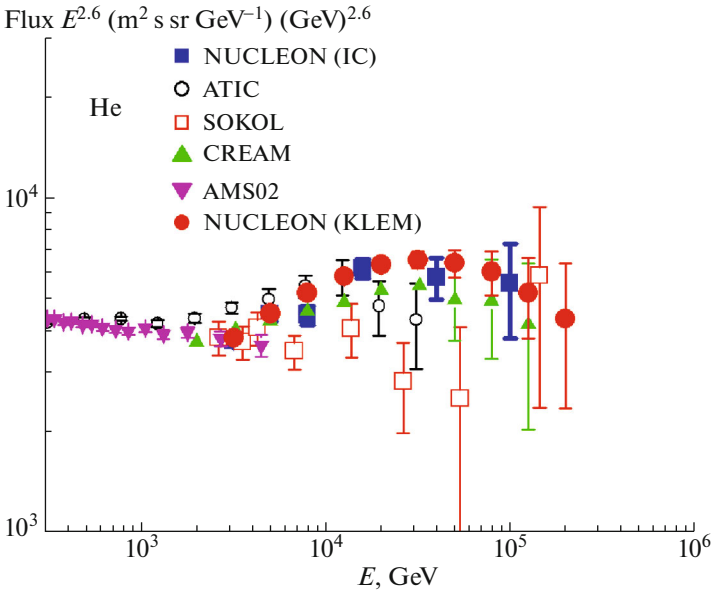

Fig. 8. (Color online) Spectrum of helium nuclei.

reconstructing the spectra. The differential spectrum of a particular cosmic-ray component is calculated as

$$\frac{dN}{d\ln E} = \frac{1}{\Gamma w W}\frac{\Delta N}{\Delta \ln(E)\Delta T}. \qquad (14)$$

In this formula, Γ is the geometrical factor of the instrument, w the fraction of live time, W the registration efficiency, ΔN the number of registered events in a bin, $\Delta(\ln E)$ the bin width on a logarithmic scale, and ΔT the total exposure time. The parameters Γ and W were determined using Monte Carlo simulations. The function $E(S)$ is non-linear. In the differential-shift method, the energy is first calculated using formula (9), then corrected using (13). Examples of artificial spectra run through the simulations and reconstructed using the method described above are presented in Fig. 6. Both a simple power-law spectrum and a spectrum with a break could be reconstructed.

In all, about 115 000 events with energies above 1 TeV were registered during the NUCLEON experiment in 2015–2017. The number of events in each

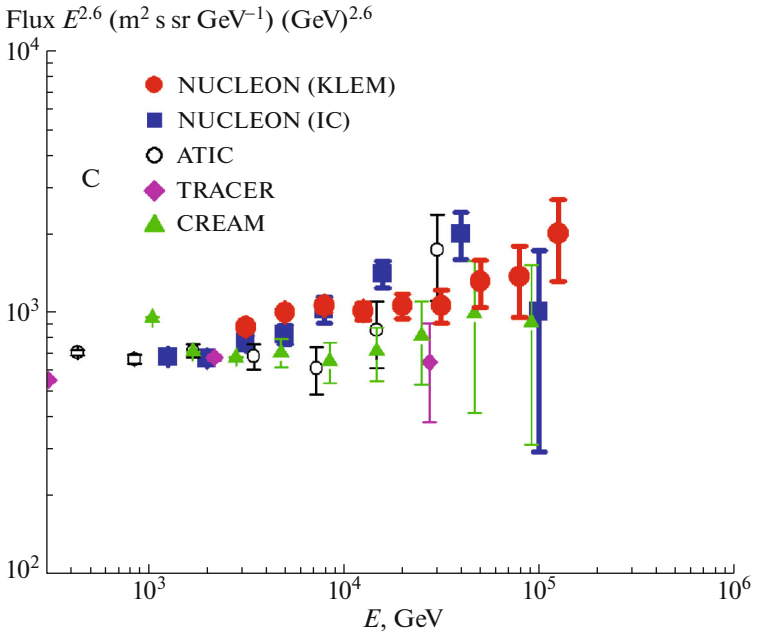

Fig. 9. (Color online) Spectrum of carbon nuclei.

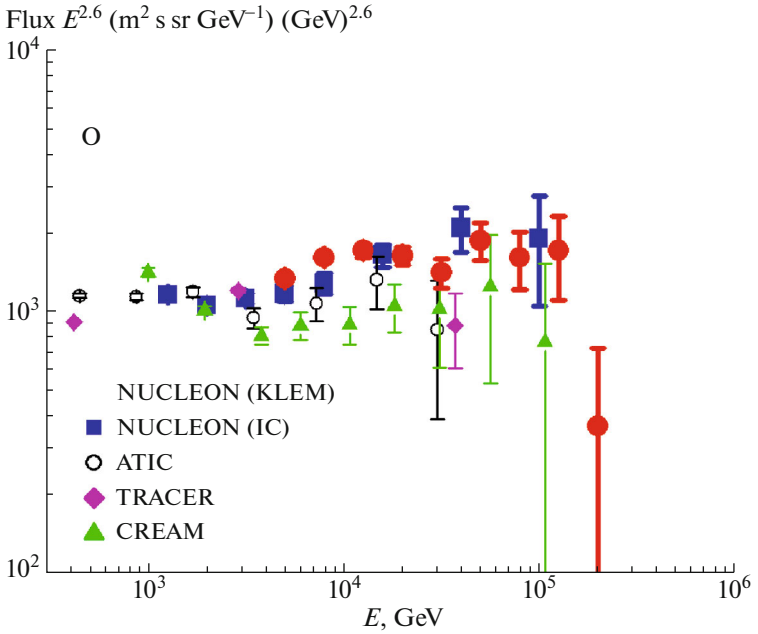

Fig. 10. (Color online) Spectrum of oxygen nuclei.

bin (ΔN) for the main abundant nuclei and the total flux of all nuclei are presented in Table 3. Note that, since different energy thresholds exist for different components, some of the bins were not used when constructing the spectra presented below.

When using the deconvolution, the deconvolution matrix [see (11)] was determined from the results of the mathematical modeling. The reconstructed particle energy was determined as a simple power-law function of the estimator S (9), and the parameters were adopted in accordance with Table 2.

A direct deconvolution was applied when reconstructing the spectra of protons and helium based on the modeling results. The spectra of other nuclei were reconstructed using the differential-shift method (see above).

Possible systematic errors could have various origins. Electron noise in the silicon detectors could lead

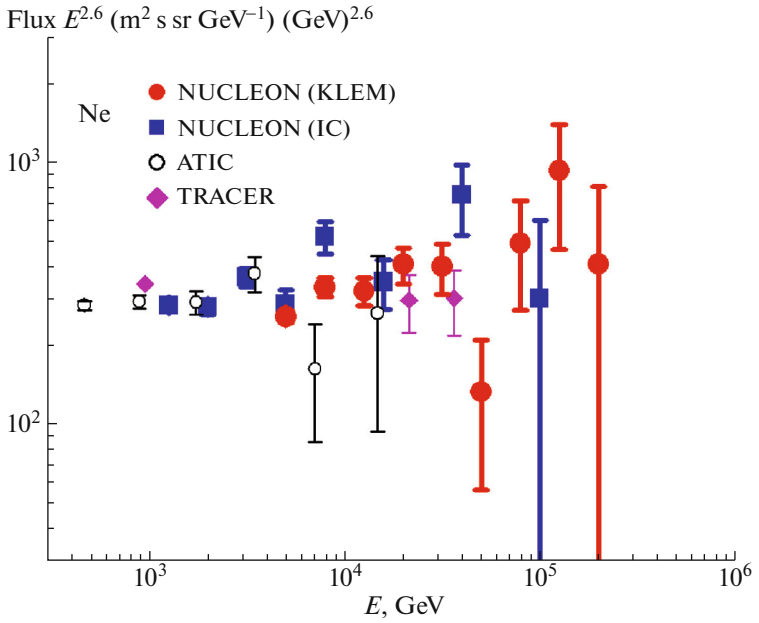

Fig. 11. (Color online) Spectrum of neon nuclei.

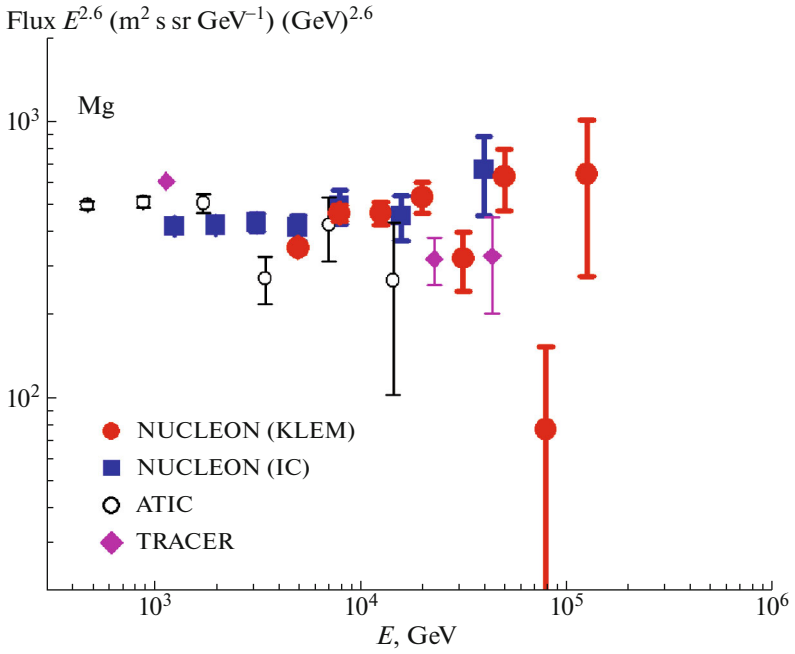

Fig. 12. (Color online) Spectrum of magnesium nuclei.

to systematic uncertainty in the energy resolution. To reduce this effect, channels with low signals (amplitudes lower than 0.5 *mip*) were rejected. The results of the mathematical modeling and the accelerator experiments were compared. The model and experimental reconstructed energy distributions were very close. The difference in the mean reconstructed energies was about 4.6% [15]. This is appreciably lower than physical fluctuations. Additional verification of the KLEM method can be carried out by comparing the reconstructed spectra with spectra obtained using traditional ionization calorimeters [2, 9, 29, 30].

The reduction of the data obtained during the in-orbit experiment were used to reconstruct the energy spectra of various cosmic-ray components. The energy spectrum for all the particles was also reconstructed [29, 30]. Figures 7–14 present spectra for abundant components (protons, helium, carbon,

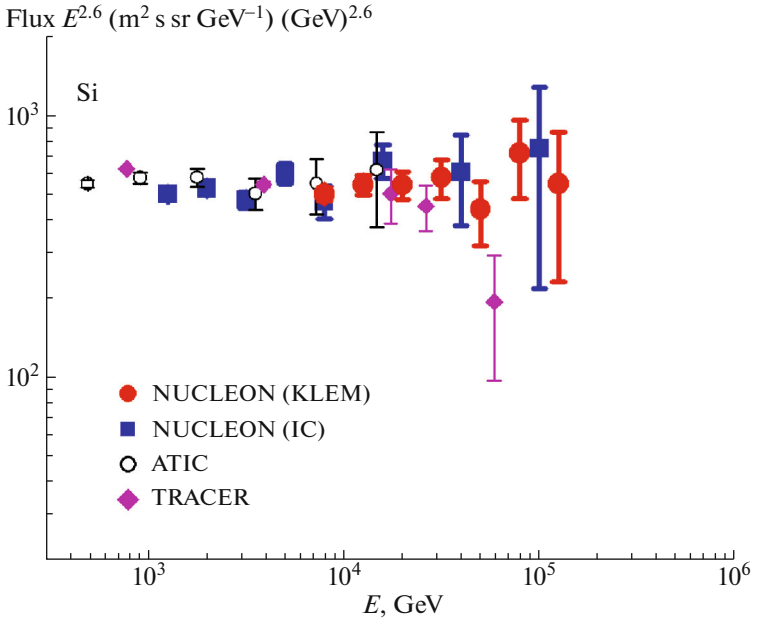

Fig. 13. (Color online) Spectrum of silicon nuclei.

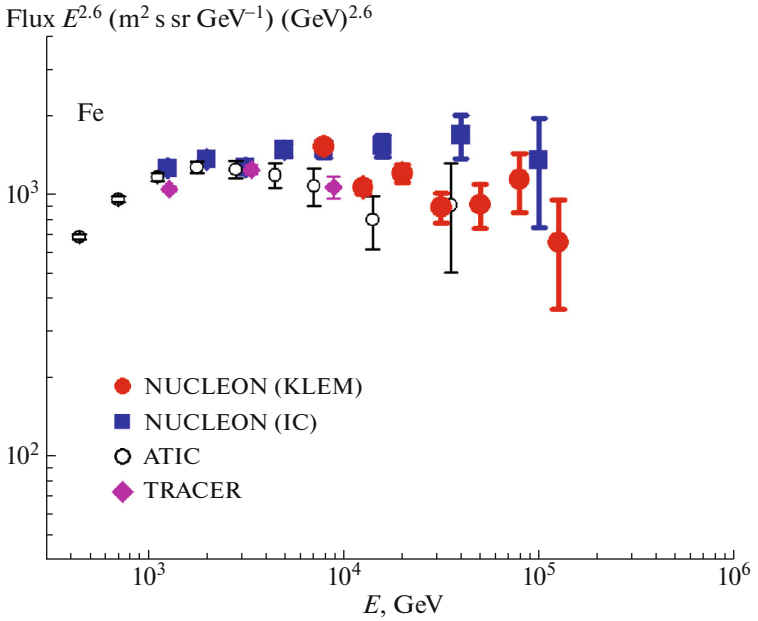

Fig. 14. (Color online) Spectrum of iron nuclei.

oxygen, neon, magnesium, silicon, iron). Spectra obtained using the KLEM method and an ionization calorimeter (IC) are shown [29, 30]. The geometrical factor for the calorimeter is substantially smaller than the geometrical factor for the KLEM detector. Only about one-fourth of the events detected by the KLEM detector were also registered by the calorimeter. Therefore, the statistical uncertainties were lower for the KLEM method than for the IC. The spectra measured in the NUCLEON experiment have been compared with the results of other experiments (ATIC [1, 2], CREAM [3, 4], TRACER [5], AMS02 [6, 7], SOKOL [8]). The spectrum of all the particles is presented in Fig. 15 and compared with various direct measurements and the high-altitude ARGO-YBJ experiment [33].

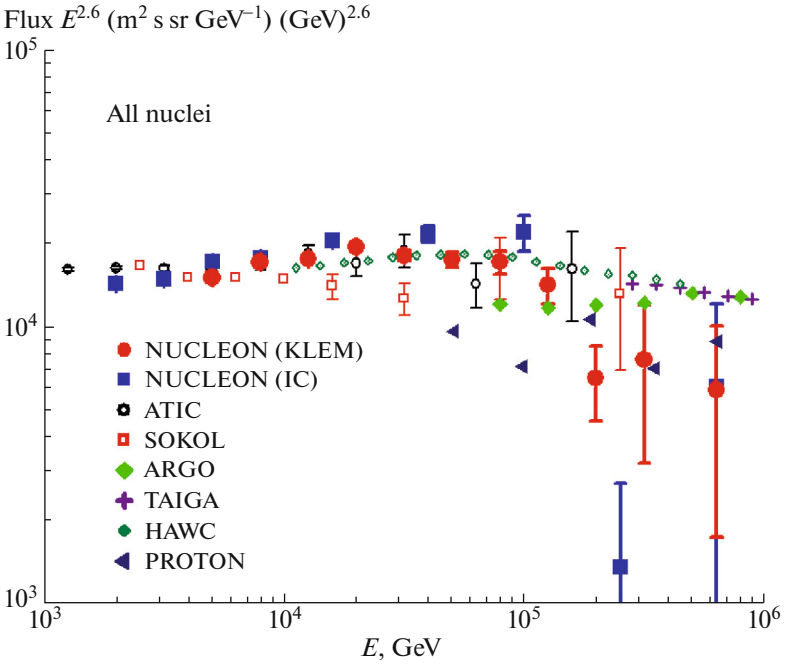

Fig. 15. (Color online) Spectrum of all particles.

6. CONCLUSION

The new KLEM method for energy measurements was tested during the NUCLEON experiment. The energy spectra obtained using different methods are in good agreement with each other. This confirms the good performance of the new KLEM method over a wide range of energies. A comparison of the energy spectra obtained using NUCLEON with the results of other experiments shows good agreement in energy ranges studied earlier. At the same time, the data for abundant nuclei from the NUCLEON experiment extend to energies above 100 TeV per particle, where no other experiments have been conducted or only poor statistics are available.

Some features are observed in some spectra of abundant nuclei (C, O, Ne, Mg) at energies of 10–100 TeV per particle (Figs. 9–13). The spectra of protons and helium nuclei have a break at a hardness of about 10 TV. These features of the spectra may be due to the presence of multiple local sources of cosmic rays [32] or of different types of sources [33].

The spectra of all particles obtained using broad atmospheric showers and direct measurements have been compared for the first time.

ACKNOWLEDGMENTS

We thank the Russian Space Agency (Roskosmos), Russian Academy of Sciences, and the Progress Rocket Space Center for support. This work was supported by the Supercomputer Center of Lomonosov Moscow State University [34].

REFERENCES

1. H. S. Ahn, E. S. Seo, O. Ganel, et al., Adv. Space Res. **37**, 1950 (2006).
2. A. D. Panov, J. H. Adams, Jr., H. S. Ahn, et al., Adv. Space Res. **37**, 1944 (2006).
3. Y. S. Yoon, H. S. Ahn, P. S. Allison, et al., Astrophys. J. **728**, 122 (2011).
4. H. S. Ahn, P. Allison, M. G. Bagliesi, et al., Astrophys. J. **707**, 593 (2009).
5. A. Obermeier, M. Ave, P. Boyle, et al., Astrophys. J. **742**, 14 (2011).
6. M. Aguilar, D. Aisa, B. Alpat, et al., Phys. Rev. Lett. **115**, 211101 (2015).
7. M. Aguilar, D. Aisa, B. Alpat, et al., Phys. Rev. Lett. **114**, 171103 (2015).
8. I. P. Ivanenko, V. Ya. Shestoperov, L. O. Chikova, et al., in *Proceedings of 23rd International Cosmic Ray Conference, Calgary, Canada, 1993* (World Scientific, River Edge, NJ, 1994), Vol. 2, p. 17.
9. P. Brogi, P. Marrocchesi, P. Maestro, and N. Mori, in *Proceedings of 34th International Cosmic Ray Conference, Hague, Netherlands,* Proc. Sci. **ICRC2015**, 595 (2016).
10. X. Wu, G. Ambrosi, R. Asfandiyarov, et al., in *Proceedings of 34th International Cosmic Ray Conference, Hague, Netherlands,* Proc. Sci. **ICRC2015**, 1192 (2016).
11. E. Atkin, V. Bulatov, V. Dorokhov, et al., Nucl. Instrum. Methods Phys. Res., Sect. A **770**, 189 (2015).
12. O. A. Vasilyev, D. E. Karmanov, I. M. Kovalyov, I. A. Kudryashov, A. A. Lobanov, D. M. Podorozhnyi, L. G. Tkachev, A. V. Tkachenko, A. N. Turundaevskiy, and V. N. Shigaev, Phys. At. Nucl. **77**, 587 (2014).

13. V. L. Bulatov, A. V. Vlasov, N. V. Gorbunov, V. M. Grebenyuk, D. E. Karmanov, A. Yu. Pakhomov, D. M. Podorozhnyi, D. A. Polkov, L. G. Tkachev, A. V. Tkachenko, S. P. Tarabrin, A. N. Turundaevskii, and S. B. Filippov, Instrum. Exp. Tech. **53**, 29 (2010).
14. A. G. Voronin, V. M. Grebenyuk, D. E. Karmanov, N. A. Korotkova, Z. V. Krumshtein, M. M. Merkin, A. Yu. Pakhomov, D. M. Podorozhnyi, A. B. Sadovskii, L. G. Sveshnikova, L. G. Tkachev, and A. N. Turundaevskii, Instrum. Exp. Tech. **50**, 187 (2007).
15. A. G. Voronin, V. M. Grebenyuk, D. E. Karmanov, N. A. Korotkova, Z. V. Krumshtein, M. M. Merkin, A. Yu. Pakhomov, D. M. Podorozhnyi, A. B. Sadovskii, L. G. Sveshnikova, L. G. Tkachev, and A. N. Turundaevskii, Instrum. Exp. Tech. **50**, 176 (2007).
16. D. M. Podorozhnyi, V. L. Bulatov, N. V. Baranova, A. V. Vlasov, A. G. Voronin, N. N. Egorov, S. A. Golubkov, V. M. Grebenyuk, D. E. Karmanov, M. G. Korolev, N. A. Korotkova, Z. V. Krumshtein, E. G. Lyannoy, M. M. Merkin, A. Yu. Pavlov, et al., Bull. Russ. Acad. Sci.: Phys. **71**, 500 (2007).
17. G. L. Bashindzhagyan, A. G. Voronin, S. A. Golubkov, V. M. Grebenyuk, N. N. Egorov, A. M. Kalinin, D. E. Karmanov, K. A. Kon'kov, N. A. Korotkova, Yu. F. Kozlov, Z. V. Krumshtein, M. M. Merkin, M. I. Panasyuk, A. Yu. Pakhomov, D. M. Podorozhnyi, et al., Instrum. Exp. Tech. **48**, 32 (2005).
18. D. M. Podorozhnyi, E. B. Postnikov, L. G. Sveshnikova, and A. N. Turundaevsky, Phys. At. Nucl. **68**, 50 (2005).
19. N. A. Korotkova, D. M. Podorozhnyi, E. B. Postnikov, T. M. Roganova, L. G. Sveshnikova, and A. N. Turundaevsky, Phys. At. Nucl. **65**, 852 (2002).
20. J. Adams, G. Bashindzhagyan, P. Bashindzhagyan, et al., Adv. Space Res. **27**, 829 (2001).
21. J. Adams, G. Bashindzhagyan, A. Chilingaryan, et al., AIP Conf. Proc. **504**, 175 (2000).
22. E. B. Postnikov, G. L. Bashindzhagyan, N. A. Korotkova, D. M. Podorozhny, T. M. Roganova, L. G. Sveshnikova, and A. N. Turundaevsky, Izv. Akad. Nauk, Ser. Fiz. **66**, 1634 (2002).
23. C. Castagnoli, G. Gortini, C. Franzinetti, A. Manfredini, and D. Moreno, Nuovo Cimento **10**, 1539 (1953).
24. R. Brun, *GEANT User's Guide,* CERN DD/EE/83/1 (Geneva, 1983).
25. N. N. Kalmykov, S. S. Ostapchenko, and A. I. Pavlov, Nucl. Phys. B (Proc. Suppl.) **52**, 17 (1997).
26. K. Batkov, G. Bigongiari, P. Maestro, P. S. Marrocchesi, M. Y. Kim, and R. Zei, Astropart. Phys. **35**, 50 (2011).
27. A. D. Panov, J. H. Adams, Jr., H. S. Ahn, K. E. Batkov, G. L. Bashindzhagyan, J. W. Watts, J. P. Wefel, J. Wu, O. Ganel, T. G. Guzik, R. M. Gunashingha, V. I. Zatsepin, J. Isbert, K. C. Kim, M. Christl, et al., Bull. Russ. Acad. Sci.: Phys. **71**, 494 (2007).
28. K. E. Batkov, A. D. Panov, J. H. Adams, et al., in *Proceedings of 29th International Cosmic Ray Conference, Pune, India, 205*, Vol. 3, p. 353.
29. E. Atkin, V. Bulatov, V. Dorokhov, et al., Astropart. Phys. **90**, 64 (2017).
30. E. Atkin, V. Bulatov, V. Dorokhov, et al., J. Cosmol. Astropart. Phys. **2017** (7), 20 (2017).
31. Zhao Yi, Jia Huan-Yu, and Zhu Feng-Rong, Chin. Phys. C **39**, 125001 (2015).
32. Y. Keum and P. Salati, Pramana—J. Phys. **86**, 369 (2016).
33. V. I. Zatsepin and N. V. Sokolskaya, Astron. Astrophys. **458**, 1 (2006).
34. V. Sadovnichy, A. Tikhonravov, Vl. Voevodin, and V. Opanasenko, in *Contemporary High Performance Computing: From Petascale toward Exascale* (Chapman Hall, CRC Comput. Sci., Boca Raton, FL, 2013), p. 283.

Translated by D. Gabuzda